Araştırma Makalesi / Research Paper
Bayburt Üniversitesi Fen Bilimleri Dergisi
Bayburt University Journal of Science

dergipark.gov.tr/bufbd
ISSN: 2667-579X

Cilt 8, Sayı 1, Yıl 2025, Sayfa 44-53
Vol 8, Issue 1, Year 2025, Pages 44-53
doi.org/10.55117/bufbd.1646880

Geliş Tarihi / Date of Recieve: 26.02.2025
Revizyon Tarihi / Date of Revision: 06.03.2025
Kabul Tarihi / Date of Acceptance: 09.04.2025

Evaluation of Casting Modulus on the Microstructure and Mechanical Properties of Spheroidal Graphite Cast Iron

Murat ÇOLAK[1], Oğuzhan ÇOLAK[2], Yasemin TABAK[3*]

[1]*Bayburt University, Engineering Faculty, Bayburt, Türkiye*
[2]*Bayburt University, Graduate Education Institute, Bayburt, Türkiye*
[3]*TUBITAK National Metrology Institute (UME), Gebze/Kocaeli, Türkiye*

Keywords:

Spheroidal cast iron, Modulus, Microstructure, Mechanical property

Abstract

Nodular graphite (Ductile) cast iron is produced by a double treatment; Nodularization / Spheroidization (Mg and/or Rare Earth) treatment + Inoculation (FeSiX-alloy treatment, with X = Ca, Ba, Sr, Ce, La, Zr etc.). Each step has specific objectives. The spheroidization of the graphite depends on the thickness of the mould and thus cooling rate is an important factor. In this work, GGG70L alloy was cast into plates that had different cross-sections. The change in the modulus has been investigated by means of microstructure and mechanical properties. It turned out that as nodule size was decreased, tensile stress and elongation at fracture were decreased however hardness was increased. It was concluded that the section thickness was an important parameter that determines the microstructure and mechanical properties of spheroidal cast irons.

*e-mail: yasemin.tabak@tubitak.gov.tr

Bu makaleye atıf yapmak için:
Murat ÇOLAK; Oğuzhan ÇOLAK; Yasemin TABAK, "Evaluation of Casting Modulus on the Microstructure and Mechanical Properties of Spheroidal Graphite Cast Iron", Bayburt Üniversitesi Fen Bilimleri Dergisi, C. 8, s 1, ss. 44-53

How to cite this article:
Murat ÇOLAK; Oğuzhan ÇOLAK; Yasemin TABAK, "Evaluation of Casting Modulus on the Microstructure and Mechanical Properties of Spheroidal Graphite Cast Iron", Bayburt University Journal of Science, vol. 8, no 1, pp. 44-53

1 INTRODUCTION

Nodular graphitic iron is characterized in a simplified way in the Fe-C-Si system. But the actual chemical composition is usually Fe-C-Si-X, with more than 30 elements present. By the addition of Ce and Mg, the graphite is converted into a spherical geometry [1]. There are several other modifiers such as Ce, Ca, Li, Na and Y, however, Mg remains as the most advantageous element for such modifications and applications [2]. The spherical geometry of the graphite enables the increase in toughness and strength to compare to the acicular lamellar graphite.

Spheroidal graphite exhibits greater strength and toughness due to the absence of tension concentration, unlike lamellar graphite's sharp ends [1] and[2]. Tensile strength, toughness, and hardness can be increased with the addition of Cu and Ni in GGG, whose mechanical properties generally vary depending on alloying element ratios. The only type of iron where heat treatment other than stress relief may be given is spheroidal graphite cast iron. By including various materials to this iron, one can strengthen its resistance to corrosion and oxidation. The tensile strength of spheroidal graphite cast iron is in the range 350 MPa – 1600 MPa [3].

The effects of spheroidal graphite cast iron, there are studies in the literature on the changes in microstructure and mechanical properties depending on the modulus change and the section thickness. Javaid and Davis [4] made studies on samples of different thicknesses. The average number of spheres reached 2500 in mm2 at 1.5 mm in thickness sample, 2200 in the 2 mm thick sample and 1300 in the 3 mm thick sample. In light of the research he studies it has been concluded that the increase in the thickness increases the average graphite diameter and the decrease in the thickness causes the number of spheres and the amount of. Doğan et al. [5] found that the number of spheres and graphite shape factor increased and the sphere size decreased as the section thickness decreased. In Bockus and Zaldarys [6] work, plates with thicknesses ranging from 3 to 50 mm were cast and microstructure studies were performed. It was concluded that the diameter of the spheres increased as the section size increased and the thickness of the section caused significant effects on the casting.

Górny and Tyrała [7] found that the hardness increased as the cross-sectional thickness decreased and the average graphite diameter decreased and the sphere diameter decreased, while the number of spheres decreased. It was observed that the globularization rate increased in direct proportion with an increasing number of spheres. Güzel et al.[8] investigated the effects of cross-sectional thickness on the hardness values and microstructure of spheroidal graphite cast iron. It was observed that the number of spheres and hardness decreased with increasing section thickness, but the sphere diameter and ferrite percentage increased. In addition, to provide high mechanical properties in GGG castings, it is stated that cross-section thickness is the key parameter. Minnebo et al.[9] show that casting defects, particularly oxides determine the tensile properties. Yeung et al.[10] looked into the solidification morphology of thin-walled casting. Pedersen and Tiedje[11] used finite difference method to convert 2D nodule count to 3D Pedersen and Tiedje[12], Park et al.[13] show that at low Mn contents, cementite is graphitized in thin sections where solidification is faster[14]. Kabnure et al.[15] researched automobile wheel casting. The samples obtained as a result of casting were examined in terms of hardness and microstructure for different cross-sectional thicknesses[16]. Combined Taguchi and Grey Relational Analysis (GRA) were used to determining the multiple response optimization of the microstructure. It has been reported that the hardness values and perlite-ferrite % increase with the decrease in the section thickness and increase in cooling speed as a result of the measurements made for cooling ratio in 6 critical regions with different cross-section thickness. Alabbasian et al.[17] examined the effect of samples of varying thickness on hardness and tensile strength values. He found that the increase in thickness caused a decrease in hardness and tensile strength. Choi et al.[18] used a step mould design to see the effect of cooling rate on graphite morphology. It was reported that rare earth addition was effective only after 2 mm thickness. Caldera et al.[19] used Y mould and found that most of the carbides were dissolved during heat treatment. Borrajo et al.[20] also used a step mould and evaluated an analytical approach between the nodule count and graphite shape factor. Abedi et al.[21] correlated the nodule count with wear properties. Shirani and Härkegård[22] used Weibull statistics to show the fatigue properties for a wind turbine. Syafaat et al.[23] characterized the wear properties of three different cast irons and found that as Mg content was increased from 0.01 to 0.3 wt%, wear volume was decreased. Azeem et al.[24] used synchrotron X-ray tomography to quantify graphite size and distribution. Tiedje et al. [25] also used 3D X-ray tomography to investigate the growth of graphites. Saito et al. [26] added Te and found that the number of graphite particles was increased. Mohammed and Kachit [27] used FEM analysis and compared the findings with experimental results. Lekakh [28] and Lekakh [29] studied the kinetics of graphite formation. Stefanescu et al. [30] has shown the effect of Ti and Mg on the morphology of cast irons.

In this study; casting of GGG70L alloy into rectangular prism shapes with different modulus, the effects of modulus replacement on the microstructure and mechanical properties of the material were investigated.

2 MATERIALS AND METHODS

In this study, the geometry and dimensions given in Figure 1 were prepared and castings were made with GGG70L alloy. Measurements of rectangular prism-shaped samples to be used in casting tests; A workpiece: 100 mm x 100 mm x 300 mm, B workpiece: 50 mm x 50 mm x 300 mm and C workpiece: 25 mm x 25 mm x 300 mm.

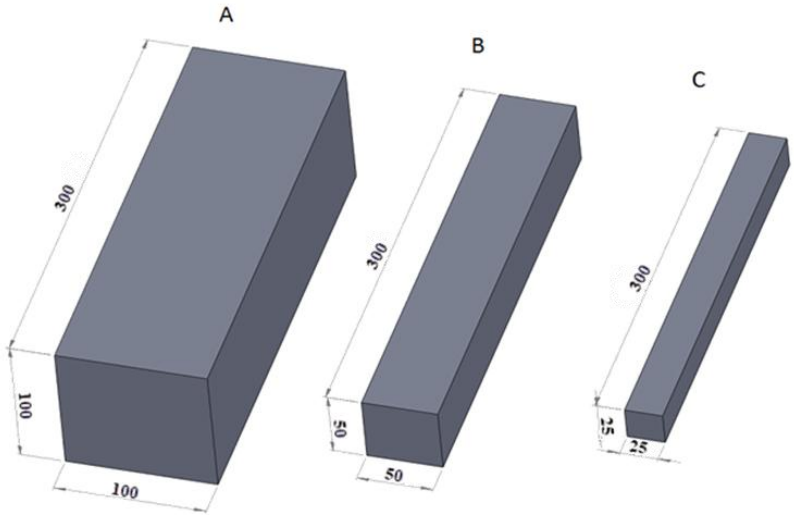

Figure 1. Geometry of the bars

The modulus values for each workpiece according to the determined dimensions were calculated by classical engineering calculation methods:

Casting modulus = Cast volume / Cast surface area

Pattern A;
M_C = (10 x 10 x 30) / [4 x (10 x 30) + 2 x (10 x 10)]
M_C = 3000 / 1400 MD = 2,1428 cm

Pattern B;
M_C = (5 x 5 x 30) / [4 x (5 x 30) + 2 x (5 x 5)]
M_C = 750 / 650 MD = 1,1538 cm

Pattern C;
M_C = (2,5 x 2,5 x 30) / [4 x (2,5 x 30) + 2 x (2,5 x 2,5)]
M_C = 187,5 / 312,5 MD = 0,6 cm

As a result of the calculations, the modulus values were found to be 2.14 cm for Sample A, 1.15 cm for Sample B and 0.6 cm for Sample C. The melting operations were carried out in an induction furnace with a melting capacity of 1000 kg (1 ton) in an industrial company operating commercially. The liquid metal taken from the furnace was spheroidized and inoculated in a pocket-type crucible. The liquid metal, which was ready for casting, was poured into a sand mold prepared to produce a sample. Samples were removed from the mold and separated from the runners and feeders and examined. Figure 2 shows the sample areas for microstructure examinations and mechanical tests from the cast sample.

2.1 Microstructural analysis

Following casting, the samples underwent metallographic preparation procedures for microstructure investigations, and an image analysis system was used to assess them. In metallographic preparation processes, the samples were initially crushed by 180, 400, 600, 800, 1000 and 1200 grit sandpaper respectively. Subsequently, it was polished with 6 µm and 3 µm diamond solution. The samples were subjected to metallographic preparation processes and after polishing, microstructure examinations were carried out with Nikon Eclipse L150-A type microscope. Photographs were taken on a Clemex digital camera connected to this microscope using Clemex Vision Lite image analysis software. Before the etching of the polished samples, microstructure examinations were performed; graphite shape factor, looked at the average sphere diameter and the spheres' percentage distribution.

Afterward, the sample was etched and the microstructure examination and percentage phase distribution after etching were determined.

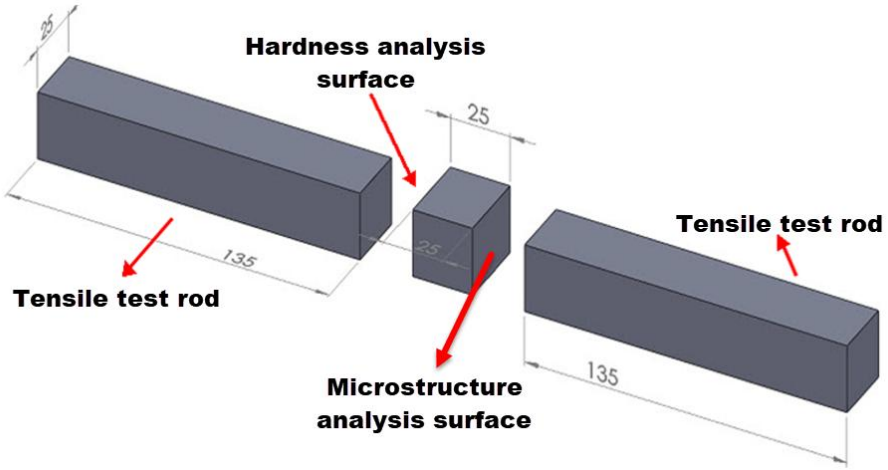

Figure 2. Sampling of the test specimens for analysis

2.2 Mechanical tests

Brinell hardness measurements of the samples obtained with the aim of determining the hardness values of our GGG 70L material were performed. STRUERS Duramin-500 brand hardness tester was used for hardness at room temperature. Two 25x25x135 mm tensile bars were removed from the cast specimens as shown in Figure 2 and machined on CNC to the required dimensions (Figure 3). Tensile testing were performed using a Zwick-Roell tensile tester at room temperature that complies with ASTM E8 standard. The scope of the study is to determine the change in mechanical values as a result of tensile tests in varying modules. Since the purpose will be only comparison, heat treatment was not applied to the tensile test samples.

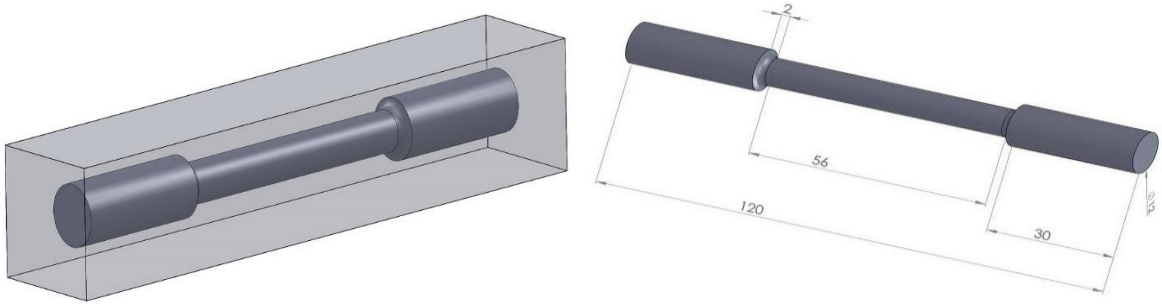

Figure 3. Tensile test bar dimension

3 RESULTS AND DISCUSSION

Table 1 provides the values associated with the chemical composition analysis findings of the samples that were taken in order to verify that the alloys used in casting tests had a suitable chemical composition. When the chemical composition values are examined, it is understood that the alloy is in the standard composition range.

Table 1. The GGG70L alloy's chemical makeup, which was used in the tests

Element	C	Si	Mn	P	S	Cr	Mo	Ni	Cu	Mg
wt %	3.36	2.38	0.5	0.03	0.01	0.019	0.44	0.72	0.56	0.05

3.1 Microstructural examination

In order to see the effects of the modulus change on the microstructure, microstructure pictures were taken at 50x, 100x and 200x magnifications from the samples taken from the castings. In Figure 4, microstructure images are given after polishing taken at 50x magnification.

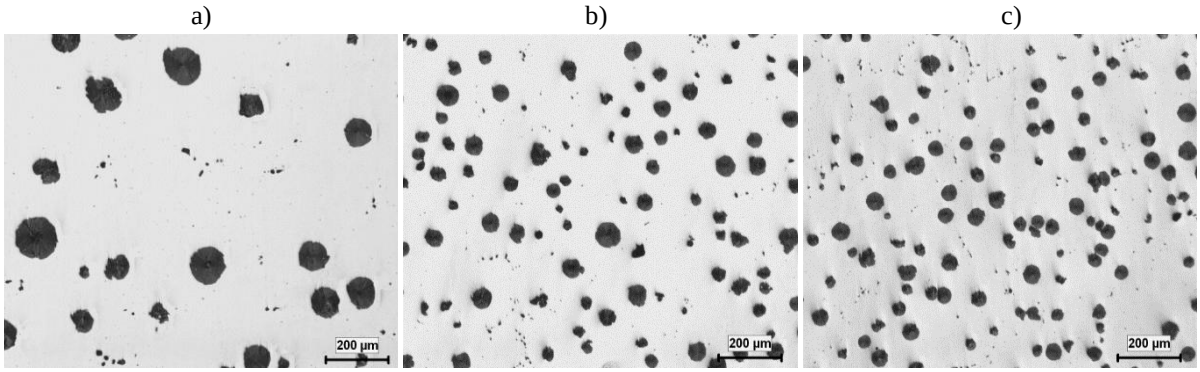

Figure 4. Microstructures of samples cast in a) Sample A (100x100), b) Sample B (50x50), c) Sample C (25x25) cross-section thickness.

As it is clearly seen in the microstructure images given in Figure 4, it is seen that the diameters of the graphite spheres are decreased due to the decrease in modulus value. Measurements of the average sphere diameter, percentage area of spheres, and graphite form factor in the internal structure of the samples were made. Measurements were performed on microstructure images taken at 100x magnification of the samples since it was found to cover a wider area and give clearer results. The average image analysis findings of many measurements taken from samples at each modulus value are displayed in Table 2. Azeem et al. [25] used 4D tool in in-situ synchrotron X-ray tomography to evaluate the graphite formation by duration for the first time. It is interesting to note that Pedersen and Tiedje [12] had carried out a 3D analysis of nodule count and compared it with 2D results. It was concluded that in thin castings, particles having a diameter less than about 5 µm should be neglected in the nodule count.

Table 2. Image analysis results of spheroidal graphite

Sample cross-section	Graphite shape factor %	Spherical radius (µm)	% graphite content	Count (100 x)
A: 100x100	84.5	38.6	10.2	112
B: 50x50	86.2	23.5	10.5	186
C: 25x25	87.4	16.3	10.6	261

In the study, the effect of microstructure on GGG production with different modulus values was investigated and the number of spheres was determined. In addition, as the cooling rate increased, the spherical values of the spheres formed more smoothly, the average sphere diameter decreased and the number of spheres per unit area increased. Stefanescu et al. [3] had reported that there was a linear correlation between cooling rate and nodule count. Abedi et al. [21] used a mould design where the thickness was ranging from 10 to 50 mm. The nodule counts were reported as 150, 220 and 450 nod/mm^2 which were very close to similar thickness results in this work as seen in Table 2.

After polishing the samples with 2% Nital solution, they were subjected to microstructure and image analysis evaluations. In Figure 5, microstructure pictures are given after etching taken at 200x magnification.

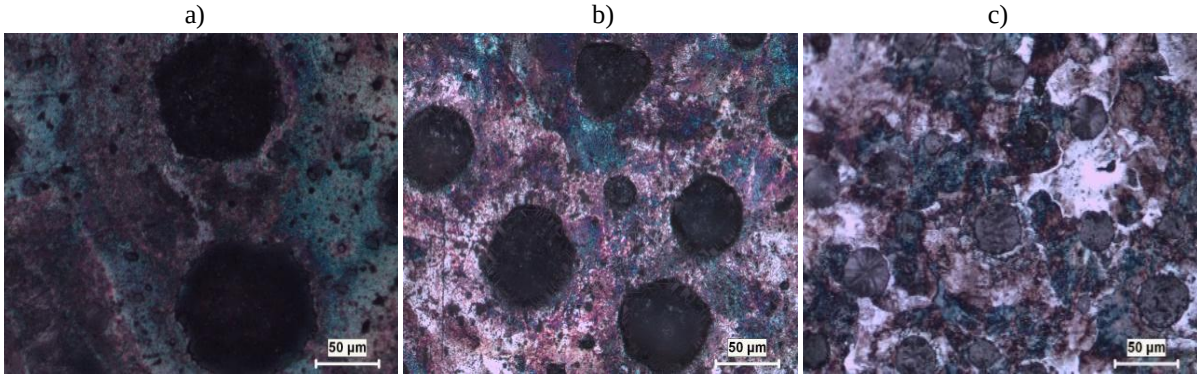

Figure 5. Microstructures of samples after etching a) Sample A (100x100), b) Sample B (50x50), c) Sample C (25x25) cross section.

When the microstructure images are examined after etching, it is understood that there are also perlite-weighted structures and ferrite and spheroidal graphite. Considering that the colour difference is more prominent and clearer results can be obtained in the image analysis studies, the studies are carried out in the pictures at 100x magnification. Table 3 shows the average phase quantities of several measurements made from samples at each modulus value. Yeung et al. (1998) suggested that in coloured metallographic analysis, directional primary austenitic dendrites were formed. Additionally, Si was found to be segregated in the core of dendrite whereas Mn was in the interdendritic locations.

Table 3. Phase analysis

Sample cross section	% Pearlite	% Ferrite	% graphite ratio
Sample A 100x100	76.5	13.1	10.2
Sample B 50x50	76.4	12.8	10.5
Sample C 25x25	77.2	12.1	10.6

When the average phase analysis values are examined and in the light of the information obtained from the studies, it is considered that the modulus change does not have a systematic and direct effect on the phase change in the structure. The change of the respective phase analysis values is mainly affected by the chemical composition of the existing samples and is thought to be related to the reduction of the size of the graphite spheres due to rapid solidification. Choi et al. [18] studied the effect of Rare Earth additions on the microstructure of ductile iron castings. It was found that in the section thickness up to 2 mm, the chilling effect was low and higher graphite count was observed. On the other hand, between 3-6 mm section thicknesses, smaller graphite with higher graphite count was recorded in the presence of rare earth where the amount of ferrite was increased.

Table 4. Tensile test results

Sample cross section	UTS (MPa)	Yield (MPa)	Elongation at fracture (%)
Sample A 100x100	620.4	504.8	5.4
Sample B 50x50	671.8	546.2	4.2
Sample C 25x25	725.2	564.6	2.6

The graphical representation of findings in Table 4 is given in Figure 6.

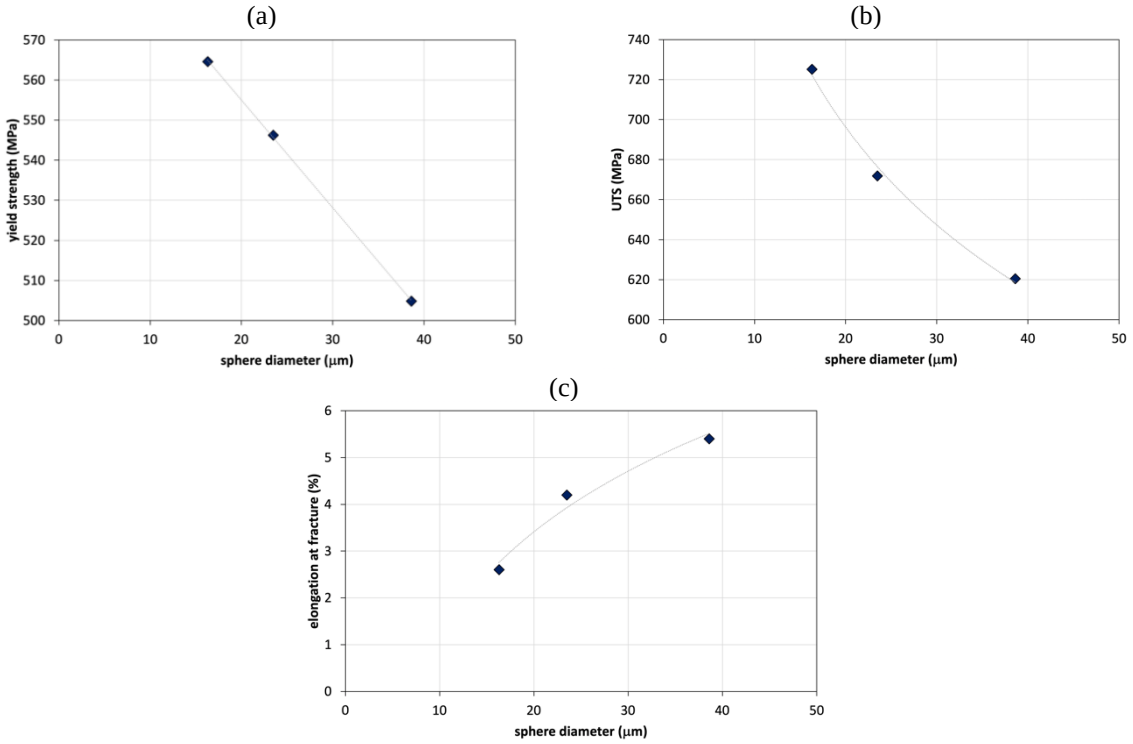

Figure 6. Results of a tensile test: (a) yield strength, (b) ultimate tensile strength, (c) elongation at fracture with regard to sphere diameter

3.2 Mechanical test results

Three tensile tests were performed from samples of different modulus A, B and C. In the evaluation of the test results, the fracture surfaces of the sample were also evaluated. In the evaluations, it was found that the surfaces were fractured from the desired area in the desired form. On the fracture surface, no porosity and inclusion was observed and it was found that the rupture was caused by metallurgical factors as expected. As a result of the studies carried out with the data obtained from the device of the samples, the tensile strength, yield strength and % elongation values of the test samples were determined (Table 4).

Figure 6 shows the clear linear relationship between yield strength and sphere diameter. However, the change in UTS is observed to be logarithmic (Figure 6b). Similarly, the elongation at fracture is exponentially increasing with increased sphere diameter. As cross-section thickness was increased, the sphere diameter was exponentially increased as seen in Figure 7. According to Alabbasian et al. [17], an increase in nodule number and nodularity in graphite, a reduction in carbide formation and lead to an increase in tensile characteristics.

When the tensile test results are examined, it is understood that the tensile strength values of the samples comply with the standards specified for the GGG70L standard sample. The tensile strength value of workpiece A with a modulus of 2.14 cm was 620.4 MPa, while the workpiece value of 671.8 MPa for workpiece B with a modulus of 1.15 cm and workpiece C of modulus 0.6 with an increase of 15% increased to 725.2 MPa It has been seen. When the effect of modulus change on the tensile test of the related alloy is evaluated, it is seen that tensile, yield strength and% elongation values decrease due to modulus change. In Figure 8, the correlation between cooling rate (modulus), UTS and elongation is given. As can be seen, with the decrease in modulus, UTS increases, and elongation decreases, visa verse for the higher modulus. Stefanescu et al. [3] had shown that the UTS and elongation was not significantly changing for the cooling rates between 5-10 K/s. Borrajo et al. [20] reported the change in cooling rate (solidification time) with different section thickness. It was found that the correlation was power fitting.

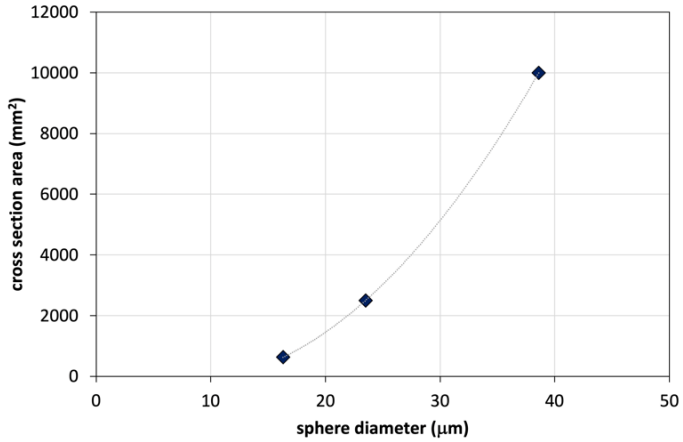

Figure7. The change in sphere diameter and cross-section thickness

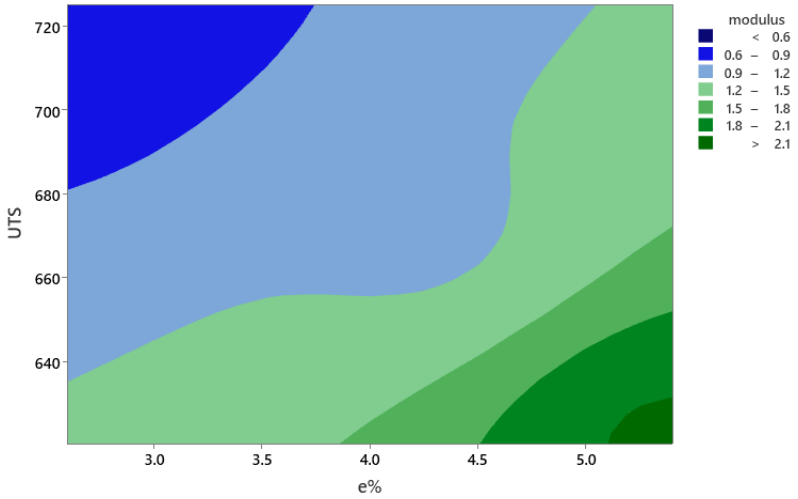

Figure 8. Correlation between modulus, UTS and elongation

3.3 Hardness test results

Hardness measurements of the samples obtained in casting tests with different modulus values were carried out in 3 seconds with 30kg load. The average hardness values of the samples taken for comparison purposes from the same regions of the cast alloys are given in Table 5. Average values were obtained by performing at least 5 measurements for related samples.

Table 5. Hardness values at different thickness

Cross-section (mm)	Average hardness (Brinell)
100 x 100	207
50 x 50	223
25 x 25	239

As given in Table 5, mean hardness values were found to be 207 BSD in A workpiece, 223 BSD in B workpiece and 239 BSD in C workpiece. The corresponding hardness values are in accordance with the GGG70L spheroidal graphite cast iron standard and are acceptable. The graphical representation in Figure 9 shows that the hardness was decreased with increased sphere diameter.

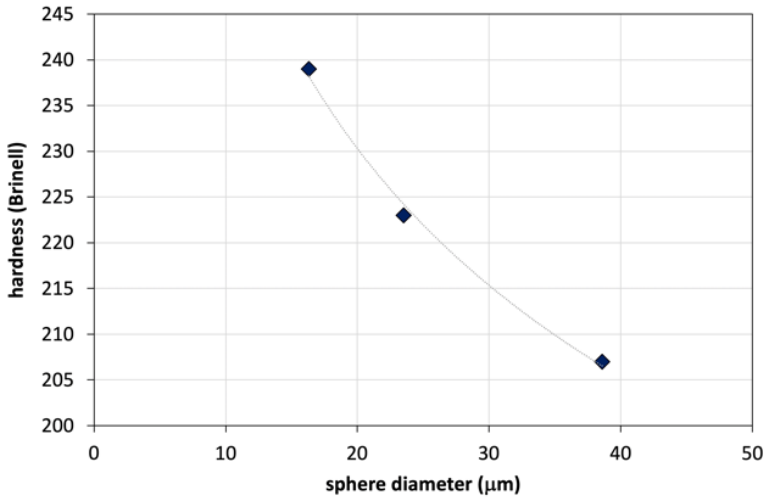

Figure 9. Change in hardness with sphere diameter

4 CONCLUSION

The results obtained from the studies on the microstructure and mechanical properties of the castings made from GGG70L alloy on rectangular prism-shaped model with three different modulus determined between 0.6 cm and 2.14 cm modulus values are given below:

- Sphericity and spheroidal graphite amount were found to vary depending on the modulus. Particularly, the spherical radius was decreased with section thickness from 38 μm to 16 μm for 25x25 to 100x100.
- The sample with a low modulus value has a smaller sphere diameter as it solidifies faster and it has been observed that the number of spheres per mm2 increases due to its rapid solidification.
- The effect of modulus size on the phase change in the structure was investigated by making image analysis evaluations after etching of samples with different modulus sizes.
- When the values obtained are considered, it is seen that the difference in modulus size does not have a decisive effect on the phase change in the structure.
- It was observed that the tensile strength of the casting samples increased exponentially from 620 MPa to 725 MPa as the modulus size decreased.
- It has been found that yield strength increases as modulus size decreases. The relationship is linear.
- It is determined that elongation at fracture value decreases logarithmically as modulus size decreases.
- The hardness values are acceptable and meet the GGG70L spheroidal graphite cast iron standard. It was found that the hardness increased as the modulus size decreased.

Acknowledgments

This research did not receive any specific grant from funding agencies in the public, commercial, or not-for-profit sectors. The authors would like to thank Dr. Derya Dışpınar from Foseco for his support in the study.

Author Contributions

Murat ÇOLAK: Conceptualization, Methodology, Software, Supervision, Project administration, Funding acquisiton
Oğuzhan ÇOLAK: Validation, Writing - Original Draft, Visualization
Yasemin TABAK: Software, Writing - Review & Editing, Visualization

All authors read and approved the final manuscript.

Conflict of interest

No conflict of interest was declared by the authors.

References

[1] S. Viswanathan and A. S. M. I. H. Committee, *ASM Handbook*, vol. 15. ASM International, 2008.

[2] J. D. Mullins, *Ductile Iron Data for Design Engineers*, 2nd ed. Montreal, Quebec: Rio Tinto Iron & Titanium, Inc., 1998.

[3] D. M. Stefanescu, L. P. Dix, R. E. Ruxanda, C. Crobitt-Coburn, and T. S. Piwonka, "Cast iron properties and applications," *AFS Trans.*, vol. 110, 2002.

[4] A. Javaid and K. G. Davis, "Microstructural analysis of cast iron," *Microsc. Microanal.*, vol. 8, no. S02, pp. 1326–1327, 2002.

[5] O. N. Dogan, K. K. Schrems, and J. A. Hawk, "Wear resistance of cast iron alloys," A*lbany Research Center (ARC)*, Albany, OR, 2003.

[6] S. Bockus and G. Zaldarys, "Structural integrity of cast iron," *Metalurgija*, vol. 48, no. 1, 2009.

[7] M. Górny and E. Tyrała, "Influence of alloying elements on cast iron properties," *J. Mater. Eng. Perform.*, vol. 22, no. 1, pp. 300–305, 2013.

[8] E. Guzel, C. Yuksel, Y. Bayrak, O. Sen, and A. Ekerim, "Hardness and wear behavior of cast iron," *Mater. Test.*, vol. 56, no. 4, pp. 285–288, 2014.

[9] P. Minnebo, K.-F. Nilsson, and D. Blagoeva, "Fatigue performance of cast iron," *J. Mater. Eng. Perform.*, vol. 16, no. 1, pp. 35–45, 2007.

[10] C. F. Yeung, H. Zhao, and W. B. Lee, "Phase transformation in cast iron," *Mater. Charact.*, vol. 40, no. 4–5, pp. 201–208, 1998.

[11] K. M. Pedersen and N. S. Tiedje, "Microstructure and properties of cast iron," *Mater. Charact.*, vol. 59, no. 8, pp. 1111–1121, 2008.

[12] K. M. Pedersen and N. Tiedje, "Measurement of cast iron microstructures," *Measurement*, vol. 41, no. 5, pp. 551–560, 2008.

[13] J. Y. Park, K. T. Choi, J. A. Szpunar, K. H. Oh, and H. Y. Ra, "Fracture mechanics of cast iron," *Scr. Mater.*, vol. 46, no. 3, pp. 199–203, 2002.

[14] Z. Ignaszak, "Heat treatment effects on cast iron," *Int. J. Cast Met. Res.*, vol. 16, no. 1–3, pp. 93–97, 2003.

[15] B. B. Kabnure and R. R. Kolhapure, "Property Optimization of Impeller Casting Using GRA," in *Int. Conf. Adv. Thermal Syst. Mater. Design Eng. (ATSMDE2017)*, 2017.

[16] V. D. Shinde, B. Ravi, and K. Narasimhan, "Numerical modeling of cast iron," *Int. J. Cast Met. Res.*, vol. 25, no. 6, pp. 364–373, 2012.

[17] F. Alabbasian, S. M. A. Boutorabi, and S. Kheirandish, "Mechanical behavior of cast iron," *Mater. Sci. Eng.* A, vol. 651, pp. 467–473, 2016.

[18] J. O. Choi, J. Y. Kim, C. O. Choi, J. K. Kim, and P. K. Rohatgi, "Wear mechanisms in cast iron," *Mater. Sci. Eng. A*, vol. 383, no. 2, pp. 323–333, 2004.

[19] M. Caldera, G. L. Rivera, R. E. Boeri, and J. A. Sikora, "Cast iron processing techniques," *Mater. Sci. Technol*., vol. 21, no. 10, pp. 1187–1191, 2005.

[20] J. M. Borrajo, R. A. Martínez, R. E. Boeri, and J. A. Sikora, "Microstructural changes in cast iron," *ISIJ Int.*, vol. 42, no. 3, pp. 257–263, 2002.

[21] H. R. Abedi, A. Fareghi, H. Saghafian, and S. H. Kheirandish, "Wear performance of cast iron," *Wear*, vol. 268, no. 3–4, pp. 622–628, 2010.

[22] M. Shirani and G. Härkegård, "Failure analysis of cast iron components," *Eng. Fail. Anal*., vol. 18, no. 1, pp. 12–24, 2011.

[23] I. Syafa'at, F. Hilmy, and M. Tauviqirrahman, "Thermal stability of cast iron," *J. Phys. Sci*., vol. 29, 2018.

[24] M. A. Azeem, M. K. Bjerre, R. C. Atwood, N. Tiedje, and P. D. Lee, "X-ray analysis of cast iron structures," *Acta Mater*., vol. 155, pp. 393–401, 2018.

[25] N. S. Tiedje, M. K. Bjerre, M. A. Azeem, and J. H. Hattel, "Cast iron properties under various cooling conditions," *Trans. Indian Inst. Met*., vol. 71, no. 11, pp. 2699–2705, 2018.

[26] R. Saito, T. Maruyama, T. Nakamura, H. Yanagitani, T. Sakai, and K. Nakamoto, "Microstructural analysis of cast iron," *Int. J. Met*., pp. 1–7, 2018.

[27] A. D. Mohammed and M. Kachit, "Mechanical testing of cast iron," *Int. J. Appl. Eng. Res.*, vol. 12, no. 5, pp. 656–663, 2017.

[28] S. N. Lekakh, "Metallurgical processing of cast iron," *Metall. Mater. Trans. B*, vol. 50, no. 2, pp. 890–902, 2019.

[29] S. N. Lekakh, "Influence of heat treatment on cast iron," *ISIJ Int*., vol. 56, no. 5, pp. 812–819, 2016.

[30] D. M. Stefanescu, G. Alonso, P. Larranaga, and R. Suarez, "Advanced cast iron processing techniques," *Acta Mater*., vol. 103, pp. 103–114, 2016.